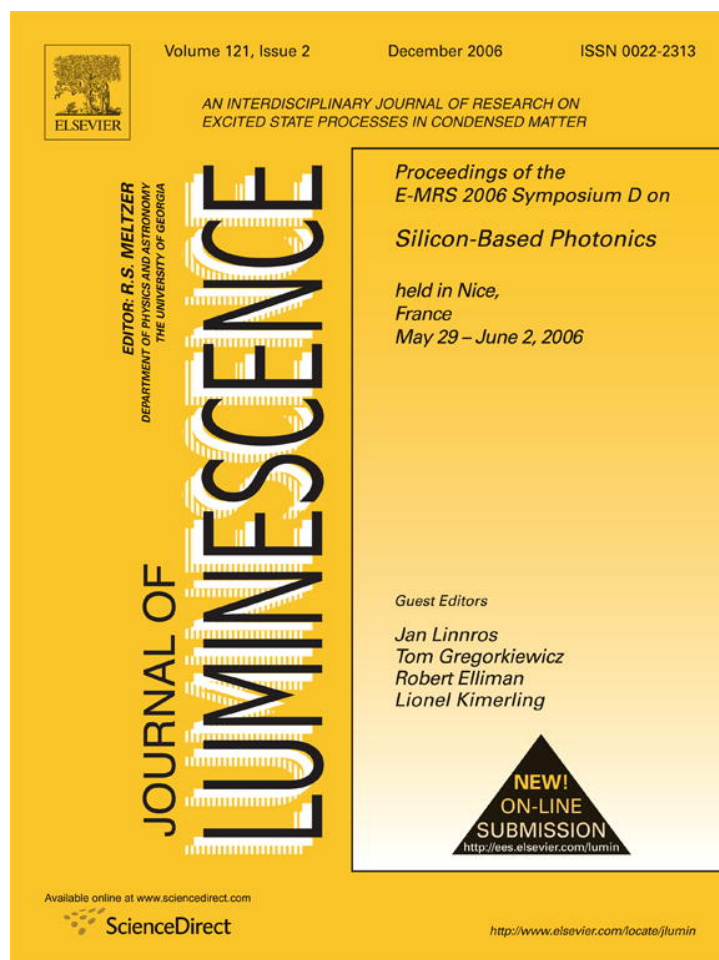


Provided for non-commercial research and educational use only.
Not for reproduction or distribution or commercial use.



This article was originally published in a journal published by Elsevier, and the attached copy is provided by Elsevier for the author's benefit and for the benefit of the author's institution, for non-commercial research and educational use including without limitation use in instruction at your institution, sending it to specific colleagues that you know, and providing a copy to your institution's administrator.

All other uses, reproduction and distribution, including without limitation commercial reprints, selling or licensing copies or access, or posting on open internet sites, your personal or institution's website or repository, are prohibited. For exceptions, permission may be sought for such use through Elsevier's permissions site at:

<http://www.elsevier.com/locate/permissionusematerial>

Optical losses and absorption cross-section of silicon nanocrystals

N. Daldosso^{a,*}, M. Melchiorri^a, L. Pavesi^a, G. Pucker^b, F. Gourbilleau^c, S. Chausserie^c,
Ali Belarouci^c, X. Portier^c, C. Dufour^c

^aDipartimento di Fisica, Università di Trento, Via Sommarive 14, I-38050 Povo (Trento), Italy

^bITC-Irst, Divisione Microsistemi, Via Sommarive 18, I-38050 Povo (Trento), Italy

^cSIFCOM, UMR CNRS 6176, ENSICAEN, 6 Boulevard Maréchal Juin, 14050 Caen Cedex, France

Abstract

Si-rich silicon oxide and SiO₂ (SRSO)/SiO₂ multilayer (ML) samples were grown by reactive magnetron sputtering and then annealed at high temperature to induce the formation of Si-nc with mean size of 3–4 nm and density of about $3.5 \times 10^{18} \text{ cm}^{-3}$ as deduced from high resolution TEM micrographs. Refractive index and thickness have been determined by m-line measurements, which have shown a birefringence of about 1.5% due to the ML structure. Rib-loaded waveguides have been fabricated to measure propagation losses in the visible–infrared range. The analysis of the different contributions to optical losses such as Mie scattering and scattering due to waveguide roughness has allowed us to isolate the contribution due to the absorption losses and thus to extract the absorption cross-section at different wavelengths. Values of about $3.5 \times 10^{-18} \text{ cm}^2$ have been found at 830 nm, increasing with decreasing of the wavelength.

© 2006 Elsevier B.V. All rights reserved.

Keywords: Absorption cross section; Silicon nanocrystals; Optical losses; Silicon photonics; Waveguides

1. Introduction

The absorption cross-section of Si nanoclusters (Si-nc) is of fundamental interest in determining the optical performance of Si-nc-based waveguides in terms of losses and achievable gain [1]. However, no clear agreement in the literature has been yet achieved, mainly because very few direct measurements have been performed [2,3]. In fact, the absorption cross-section of Si nanostructures is usually deduced from the effective excitation cross-section measured by photoluminescence lifetimes often referred to very short wavelength such as 365 or 488 nm [4–7]. This is not so interesting from the light propagation point of view: in fact, light emission in Si-nc cover the range 600–900 nm depending on the Si-nc size and surface passivation.

In this paper, we present direct measurements of the absorption cross-section by performing optical transmission experiments in rib-loaded waveguides containing Si-nc of different sizes and densities, thus measuring the

propagation losses and consequently the absorption cross-sections once the Si-nc density is determined by high-resolution TEM images.

2. Sample growth and characterization

Si-rich silicon oxide (SRSO)/SiO₂ multilayers (MLs) have been grown by reactive magnetron sputtering of a pure silica target. The use of pure argon in the plasma leads to the deposition of a silica sublayer, whereas the injection of argon and hydrogen mixture allows the growing of a SRSO sublayer due to the ability of hydrogen to reduce the oxygen species resulting from the target sputtering. ML structure is then achieved through the alternation of pure Ar and Ar/H₂ plasma. MLs have been deposited on a (0 0 1) Si substrate on which a 3 μm-thick SiO₂ buffer layer was previously deposited. Different samples, consisting of a sequential alternation of SRSO and SiO₂ sublayer thicknesses, have been produced. In this work, we report on two specific samples with parameters given in Table 1. More details about the process can be found elsewhere [8]. After

*Corresponding author. Tel.: +39 0461882030; fax: +39 0461881696.
E-mail address: daldosso@science.unitn.it (N. Daldosso).

Table 1

Deposition parameters, core layer refractive index and thickness by m-line measurements; SiO₂ layer thickness, Si-nc mean size and density as obtained by TEM measurements

Sample	Deposition parameters	n_{core} (TE) at 633 nm	Core thickness (μm)	SiO ₂ thickness (μm)	Si-nc size (nm)	Si-nc density (10^{18}cm^{-3})
A	60 [SRSO/SiO ₂]	1.776	1.02 ± 0.01	15.5 ± 0.5	4 ± 0.5	3.4 ± 0.9
B	50 [SRSO/SiO ₂]	1.565	1.88 ± 0.01	31.5 ± 0.5	3 ± 0.5	3.5 ± 1.2

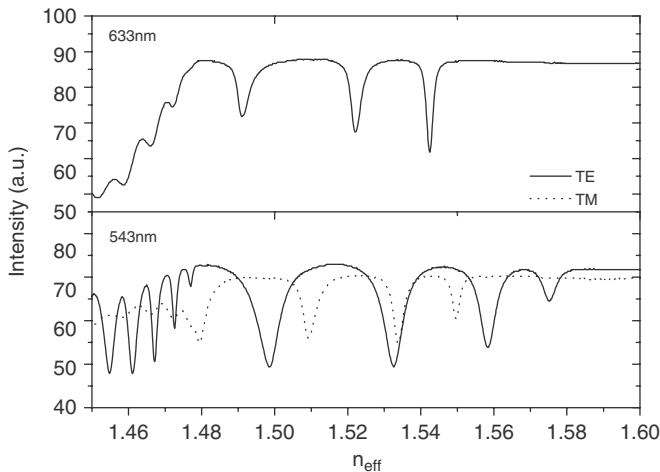


Fig. 1. Sample B: m-line measurements performed at 633 and 543 nm.

deposition, each sample has been annealed for 1 h at 1080 °C under a pure nitrogen flux.

To characterize the optical properties of the samples, m-line measurements have been performed at 633 and 543 nm, respectively (Fig. 1). The main results about core layer refractive index (for TE polarization) and thicknesses are reported in Table 1. The measured modal refractive indices n_{TE} and n_{TM} can only be explained by a negative “form birefringence” of about 1.5% originating from the particular structure of the active core, i.e. a periodical set of parallel planes of two different materials. Light polarized parallel to the layers (TE-polarization) experiences the ordinary refractive index n_o , which is higher than the extraordinary refractive index n_e experienced by light polarized perpendicular to the layers (TM-polarization). Therefore, a negative material birefringence, defined as $\beta(\%) = 100(n_e - n_o)/n_o$, has been found. The values of birefringence found here are comparable with other previous results obtained in similar structures [9].

The SRSO sublayers have been deposited under specific conditions described elsewhere [8], allowing the highest incorporation of Si excess. In this context, one can suppose that the thickness of the SRSO sublayer gives the size of the Si grain which is assumed to be spherical [8]. In fact, for sample B the thickness of the SRSO sublayer results, after the thermal annealing, in Si-nc sizes of 3 ± 0.5 nm as measured from HRTEM (high resolution transmission electron microscopy) images which have been performed to determine both the SRSO sublayer, i.e. the Si-nc size, and the SiO₂ sublayer thicknesses. Results are shown in

Table 1. It is worth noting that the measured values are in agreement with the total core layer thickness determined by m-line measurements: i.e. for sample A, 1170 ± 60 nm from TEM and 1020 ± 20 nm from m-line, respectively. Fig. 2 shows HRTEM images for sample A and B, respectively. One can appreciate the perfect stacking of each sublayer that can be achieved with such reactive process. The introduction of hydrogen in the plasma favours the incorporation of a Si excess and the formation of a thick enough sublayer, i.e. larger than 2 nm, of Si nanocrystals as evidenced in the HRTEM micrographics. Si-nc densities of about $3.5 \times 10^{18} \text{cm}^{-3}$ are obtained (last column in Table 1).

3. Waveguide fabrication

Optical lithography and reactive ion etching were used to define rib-loaded waveguides. The photolithographic mask used for waveguide definition consisted of approximately 500 lines 4 cm long and with different rib widths. Samples were cut and the facets polished to favour light injection: waveguide length was 0.5 cm for sample A and 0.3 cm for sample B.

Atomic force microscopy (AFM) was performed to check the resulting waveguide structure and to characterize the surface roughness: values of about 6.5 ± 0.5 nm have been obtained for both samples. These values are not very high, suggesting that the fabrication process allows a good control of the layer deposition and processing. In fact, the surface roughness values are not very different from those obtained before the etching process. The rib width as measured from AFM resulted in about 12 μm for the largest waveguides, which are those used for optical transmission measurements.

4. Optical transmission measurements

Propagation loss coefficients have been obtained by the insertion loss (IL) technique. IL measurements have been performed by using the light of a He–Ne laser (632.8 nm; 10 mW), of various diode lasers (655 nm, 10 mW; 785 nm, 13 mW and 830 nm, 15 mW) and of a tunable laser (1260–1630 nm; 3 mW) coupled into the waveguides through a single mode tapered fibre. IL technique is based on the measurement of the power transmitted from the waveguide output facet as a function of the input signal power. IL count for coupling losses and propagation ones. The losses through the optical collection system

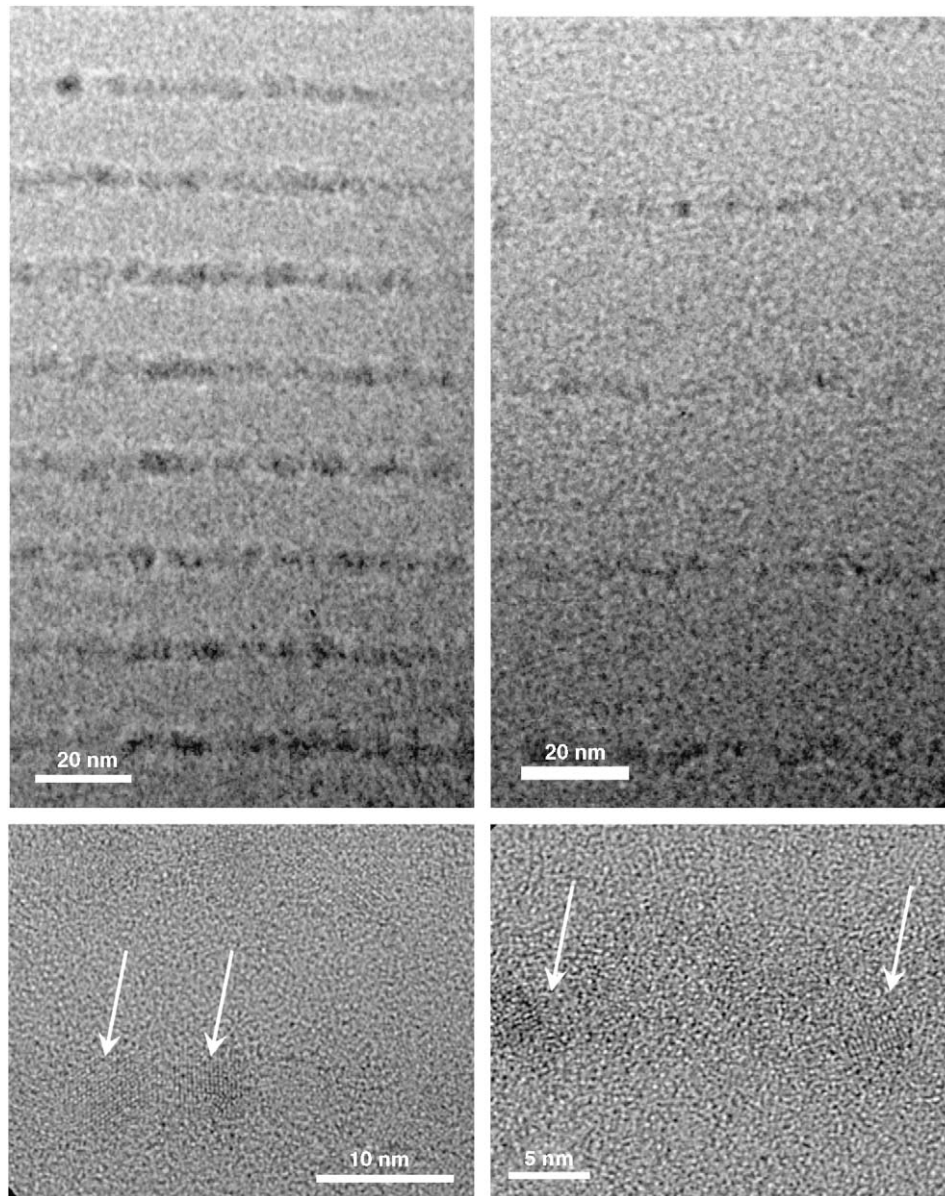


Fig. 2. HRTEM images for sample A (left panels) and sample B (right panels).

(coupling-out losses) have been determined by measuring the transmitted power of the tapered fibre in front of the collecting microscope objective. The coupling-in losses have been calculated by an estimation of several effects. The reflection on the waveguide facet accounts for about 0.2 dB for all wavelengths. Non-perfect coupling between tapered fibre and input facet accounts for about 1 dB (calculated for 6 μm of separation and for 1° of axial misalignment). By considering a Gaussian input laser beam, the difference between tapered fibre's spot size (5 μm in the near-infrared range and about 15–20% smaller in the visible) and optical waveguide mode size accounts for around 6–7 dB in the visible and 7–8 dB in the near-infrared range. No losses due to the different numerical aperture (NA) are present (NA of the waveguide is larger than the one of the input fibre for all the wavelengths we

used). Therefore, a conservative estimate of the coupling-in losses is not less than 8 dB in the visible and not less than 9 dB in the near-infrared range. Subtracting the estimated coupling losses from the IL measurements, the propagation losses can be obtained. Propagation loss coefficients of the different waveguides at various wavelengths for the largest rib width (about 12 μm) are reported in Table 2. In sample A, coupling in losses are slightly smaller because of a smaller fibre spot size but nevertheless no transmitted signal at 632.8 and 655 nm has been measured because of large losses.

Optical guided modes have also been observed in the near-infrared range (1260–1630 nm), where the Si-nc are transparent and thus absorption losses are negligible. Fig. 3 shows the IL measurements of sample B: propagation losses decrease with increasing wavelength. Propagation

Table 2
Propagation losses at different wavelengths

Sample	Propagation losses (dB/cm)				
	633 nm	655 nm	785 nm	830 nm	1630 nm
A	—	—	—	70 ± 4	14 ± 2
B	136 ± 5	127 ± 5	73 ± 5	57 ± 4	2 ± 2

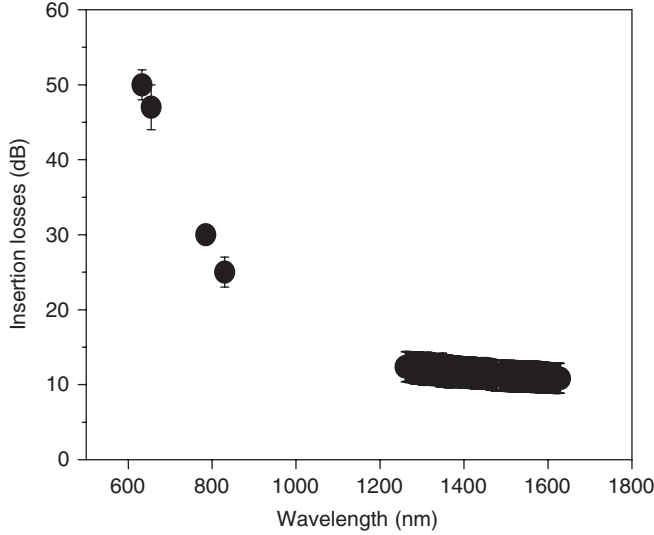


Fig. 3. Insertion loss measurements as a function of the wavelength in waveguide sample B.

loss coefficients at 1630 nm are also reported in Table 2 for both samples. It is worth noting here that sample A presents a quite larger value with respect to sample B. We will discuss this point in the following.

5. Optical losses discussion

Various mechanisms contribute to optical losses in rib-loaded waveguides. In general, propagation losses of a waveguide mainly come from light scattering due to the inhomogeneous nature of the core layer (Si nanoparticles of nm dimensions embedded in amorphous silica), waveguide roughness and absorption losses: $\alpha_{prop.} = \alpha_{Mie-scatt.}(\lambda) + \alpha_{roughness}(\lambda) + \alpha_{abs}(\lambda)$. By considering a nanocrystal of radius a , we can calculate the Mie scattering loss contribution ($\alpha_{Mie-scatt.}$) by using [10]

$$\alpha_{Mie-scatt.}(\lambda) = \sigma_{Mie-scatt.}(\lambda) N_{Si-nc}$$

$$= \frac{8\pi}{3} N_{Si-nc} \left(\frac{2\pi n_{SiO_2}}{\lambda} \right)^4 a^6 \left(\frac{m^2 - 1}{m^2 + 2} \right)^2, \quad (1)$$

where N_{Si-nc} is the Si-nc density, n_{SiO_2} the SiO₂ refractive index and m the ratio of the refractive index between Si and SiO₂.

The roughness contribution $\alpha_{roughness}$ is expressed as [11]

$$\alpha_{roughness}(\lambda) = \frac{16\pi^3 n_{core}^2 \rho^2 \cos^3 \theta}{\sin \theta \left(\frac{1}{\sqrt{n_{eff}^2 - n_2^2}} + \frac{1}{\sqrt{n_{eff}^2 - n_1^2}} \right)} \times \left[\frac{1}{\lambda_0^3 + \frac{2\pi t_{core}}{\left(\frac{1}{\sqrt{n_{eff}^2 - n_2^2}} + \frac{1}{\sqrt{n_{eff}^2 - n_1^2}} \right)} \lambda_0^2} \right], \quad (2)$$

where ρ is the surface roughness, $\sin \theta = n_{eff}/n_{core}$ is the modal propagation angle within the waveguide, t_{core} the core thickness, n_{eff} the modal effective index and n_1 and n_2 are the refractive indices of the upper and bottom claddings, respectively. The losses due to sidewall roughness have not been taken into account because of a negligible interaction between optical mode and sidewalls due to the large rib width (about 12 μm) and the high modal confinement factor (very close to 1).

Having determined refractive indices and thicknesses by m-line measurements, surface roughness by AFM, and Si-nc mean size and density by TEM image analysis, it is straightforward to calculate losses due to Mie scattering and surface roughness by means of Eqs. (1) and (2), respectively.

Mie scattering at 633 nm accounts for about 1.5 dB/cm (sample A) and 0.3 dB/cm (sample B) and for less than 0.5 and 0.1 dB/cm at 830 nm, respectively. Roughness losses range from about 1 dB/cm for sample B up to 3 dB/cm for sample A.

For sample B the loss coefficients obtained at 1600 nm (where absorption of Si-nc is absent) well matches the sum of Mie and roughness scattering losses. Whereas this is not the case for sample A: we argue that, due to internal macroscopic defects of the waveguide, another loss contribution α_{wg} can be taken into account. In a first order approximation we assume α_{wg} to be wavelength independent.

By using the computed $\alpha_{Mie-scatt.}$ (Eq. (1)) and $\alpha_{roughness}$ (Eq. (2)), the absorption loss coefficients α_{abs} can be obtained from the measured α_{prop} data (see Fig. 4 where also the absorption cross-sections are reported: $\sigma_{abs} = \alpha_{abs}/N_{Si-nc}\Gamma$). The modal confinement factor Γ is about 1 for visible wavelengths as shown by simulations taking into account the optical thickness and the waveguide geometry. Absorption cross-sections of about $3.5 \times 10^{-18} \text{ cm}^2$ have been found at 830 nm for both samples, independent of the total amount of propagation losses. Small difference due to different sizes cannot be appreciated here. Very similar samples with quite different sizes are needed to investigate a possible trend on σ_{abs} as a function of Si-nc size.

It is worth noting that σ_{abs} decreases as a function of the wavelength (sample B) due to a decrease of the Si-nc absorbance in the range 400–1100 nm as expected [12]. Unfortunately, no optical transmission at shorter wavelengths (i.e. 514 or 488 nm) has been detected due to the

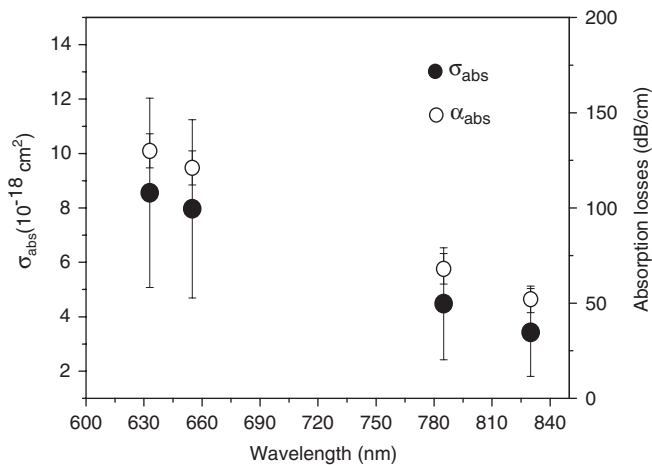


Fig. 4. Absorption losses α_{abs} (empty symbols) and absorption cross-sections (full symbols) $\sigma_{\text{abs}} = \alpha_{\text{abs}}/N_{\text{Si-nc}}\Gamma$ of sample B at different wavelengths. Sample A measured at 830 nm reports the same data within the error bar.

very large losses, thus preventing any direct comparison with values obtained from lifetime measurements.

The σ_{abs} values found in this paper are quite in agreement with other results. In Ref. [13] values around 10^{-19} cm^2 have been estimated at 785 nm for Si-nc slab waveguides by supposing a Si-nc density of about $2 \times 10^{19} \text{ cm}^{-3}$, whereas in Ref. [3], ion-implanted Si-nc waveguides with measured Si-nc density of $2 \times 10^{19} \text{ cm}^{-3}$ and Si-nc size of about 4 nm showed σ_{abs} of about $5 \times 10^{-19} \text{ cm}^2$ at 780 nm. It is worth noting that a factor of 2 or 4 in the estimation of the Si-nc density could fill the difference with our data.

6. Conclusion

Rib-loaded waveguides containing Si nanocrystals have been fabricated and characterized in terms of structural parameters such as Si-nc size and density and in terms of optical losses. Thanks to the determination of the roughness, waveguide scattering has been evaluated as well as

Mie scattering, thus allowing the determination of absorption losses as a function of the wavelength. Absorption cross-section was thus obtained, resulting in about $3.5 \times 10^{-18} \text{ cm}^2$ at 830 nm and about $8.5 \times 10^{-18} \text{ cm}^2$ at 633 nm, typical wavelength for optical gain of these materials. These numbers are of fundamental importance for the feasibility of a high performance optical amplifier that makes use of similar optimized structures.

Acknowledgements

We thank Dr. D. Navarro-Urrios for m-line measurements. Financial support by EC under Projects FP6-017158-PHOLOGIC and FP6-505285-SEMINANO is acknowledged.

References

- [1] L. Pavesi, D. Lockwood (Eds.), Silicon Photonics, Topics in Applied Physics, vol. 94, Springer, Berlin, 2004.
- [2] L. Khriachtchev, M. Räsänen, S. Novikov, Appl. Phys. Lett. 83 (2003) 3018.
- [3] P. Pellegrino, B. Garrido, C. Garcia, J. Arbiol, J.R. Morante, M. Melchiorri, N. Daldosso, L. Pavesi, E. Schedi, G. Sarrabayrouse, J. Appl. Phys. 97 (2005) 074312.
- [4] D. Kovalev, J. Diener, H. Heckler, G. Polisski, N.K. Sunzner, F. Koch, Phys. Rev. B 61 (2000) 4485.
- [5] F. Priolo, G. Franzò, D. Pacifici, V. Vinciguerra, J. Appl. Phys. 89 (2001) 264.
- [6] L. Khriachtchev, Appl. Phys. Lett. 81 (2002) 1357.
- [7] C. Garcia, B. Garrido, P. Pellegrino, R. Ferré, J.A. Moreno, L. Pavesi, M. Cazzanelli, J.R. Morante, Physica E 16 (2003) 429.
- [8] C. Ternon, F. Gourbilleau, X. Portier, P. Voivenel, C. Dufour, Thin Solid Films 419 (2002) 5.
- [9] D. Navarro-Urrios, F. Riboli, M. Cazzanelli, A. Chiasera, N. Daldosso, L. Pavesi, C.J. Oton, J. Heitmann, L.X. Yi, R. Scholz, M. Zacharias, Opt. Mater. 27 (2005) 763.
- [10] A.J. Cox, A.J. De Weerd, J. Linden, Am. J. Phys. 70 (2002) 620.
- [11] F.P. Payne, P.R. Lacey, Opt. Quantum Electron. 26 (1994) 977.
- [12] R.G. Elliman, M.J. Lederer, B. Luther-Davies, Appl. Phys. Lett. 80 (2002) 1325.
- [13] L. Khriachtchev, Appl. Phys. Lett. 81 (2002) 1357.